Available online at www.sciencedirect.com

ScienceDirect

journal homepage: www.elsevier.com/locate/he

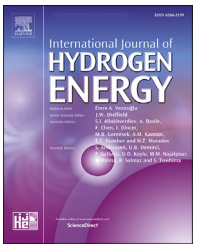

Hydrogen flow rate control in a liquid organic hydrogen carrier batch reactor for hydrogen storage

Marco Gambini, Federica Guarnaccia, Michele Manno[*], *Michela Vellini*

University of Rome Tor Vergata, Via del Politecnico, 1, Rome, 00133, Italy

HIGHLIGHTS

- Liquid Organic Hydrogen Carriers release hydrogen at highly variable flow rates
- Flow rate control systems are required to meet end-user demand
- Control variables: discharge pressure, thermal fluid inlet temperature and flow rate
- Heat transfer fluid inlet temperature provides the most effective control
- Very good controllability expected with synergic pressure and temperature controls

ARTICLE INFO

Article history:
Received 1 March 2023
Received in revised form
9 May 2023
Accepted 14 May 2023
Available online 1 June 2023

Keywords:
LOHC
Hydrogen storage
Lumped-parameter model
Power control
Heat transfer

ABSTRACT

Liquid Organic Hydrogen Carriers (LOHCs) feature a highly variable rate of hydrogen release if held at constant pressure and temperature, but in real-life applications hydrogen release must be controlled to match end-user demand. The aim of this paper is to provide an overall assessment of LOHC systems' controllability, within a general framework regardless of the specific application field. Hydrogen discharge can be controlled through the reactor pressure and temperature; thus, a PI controller is introduced acting on three control variables independently: discharge pressure; thermal fluid inlet temperature; thermal fluid mass flow rate. A quantile analysis is performed on the uncontrolled hydrogen release: practical values of the energy-to-power ratios for LOHC systems are 2–6 h. A normalised release time is introduced to assess the efficiency of the control system. Temperature control leads to the best results, with an efficiency higher than 90% for the entire load range, while pressure control leads to satisfactory performance only at low loads. The mass flow rate control is the least effective, with efficiencies always below 80%. Sensitivity analysis highlights the temperature control strategy as the best fit to enhance controllability across the whole power range. Pressure control presents a more variable trend.

Introduction

The need to reduce carbon emissions is driving a paradigm shift in power production. The International Energy Agency forecasts a 2400 GW growth in renewable power capacity over the 2022–2027 period [1]. Increasing by 10% points, renewables are expected to become the largest source of global electricity generation. The new installed capacity will be

* *Corresponding author.*
E-mail addresses: gambini@ing.uniroma2.it (M. Gambini), federica.guarnaccia@students.uniroma2.eu (F. Guarnaccia), michele.manno@uniroma2.it (M. Manno), vellini@ing.uniroma2.it (M. Vellini).

https://doi.org/10.1016/j.ijhydene.2023.05.153

mainly due to solar photovoltaic and wind technologies, while dispatchable renewables, such as bioenergy and hydropower, will still be limited. As such, there is a growing need for additional power sources to increase the flexibility of the system. Demand-side management can lower storage requirements; however, electricity networks can only account for spatial but not temporal balancing. Flexible energy generation routes and alternative energy storage solutions are needed to counteract wind and solar intermittency [2].

For this purpose, Power-to-X has emerged as a pathway to make use of excess renewable conversion. Green fuels and chemicals are thus produced for subsequent dispatch, even allowing for decarbonisation in hard-to-abate sectors [2,3]. Power-to-hydrogen (P2H) may provide grid balancing services and long-term storage, accounting for variations in the power supply from wind and solar technologies [4]. As such, it could play a key role in increasing the share of Renewable Energy Sources (RES) in the power sector [5]. Clean hydrogen produced from RES could also be used as feedstock as a green precursor for ammonia and methanol [4,6]. Hydrogen production constitutes the main cost element of P2H: by 2035, the levelized costs of green hydrogen production technologies are expected to be around 3.2–4.8 GBP/kg [7] mainly due to CAPEX expenses [8]; however, green hydrogen could be economically competitive with fossil fuel-derived hydrogen by 2030 in regions with abundant and inexpensive renewable electricity [9].

Hydrogen must be stored and distributed to a variety of applications in a fully developed decarbonised energy system based on P2H and Hydrogen-to-X technologies [10]. Despite a high energy density when compared to its mass (120.0 MJ/kg [11]), its low volumetric density (0.084 kg/m^3 at normal pressure and temperature) requires a process to increase the storage density, considerably adding to the final cost. Compression is currently the cheapest option (about 0.5 GBP/kg [7]), but also provides the lowest density improvement: density is about 40.0 kg/m^3 at 700 bar and 288 K [12]. The other traditional route is liquid hydrogen (LH_2), which is currently being evaluated as a potential vector in the transportation sector [13]. With respect to gaseous hydrogen, its density is about 80% higher: 70.8 kg/m^3 at 1 atm and 20 K [14]. However, LH_2 is expensive (forecast at about 1.9 GBP/kg by 2035 [7]) and is thus mainly used in special applications where high-purity hydrogen is needed (such as rocket fuel or chip-making industry). Moreover, due to boil-off, up to 15% of the stored hydrogen can be lost daily [15] in relatively small refuelling stations (100 kg/d of hydrogen delivered). Liquid Organic Hydrogen Carriers (LOHCs) are one of the most promising alternative options to compressed or liquefied hydrogen [16], and are considered a potential enabler of P2H technologies in the long term [10]. Even if a continent-wide system of hydrogen pipelines is considered to transport hydrogen from production facilities [17], other means to store and transport hydrogen are necessary to reach unconnected end-use locations. Conversion of LOHCs should add an additional 0.9 GBP/kg to the P2H chain (compared to the 1.4 GBP/kg increase related to the conversion of ammonia [7]), but higher volumetric densities are allowed.

LOHCs can be divided into two main categories: (1) homocyclic compounds: first introduced as simple aromatic compounds such as benzene and toluene in the early 1980s, most research now mainly focuses on cycloalkanes and polycyclic alkanes [18]; (2) heterocyclic compounds such as O-containing molecules (such as ester/alcohol pairs) and N-containing molecules (such as N-heterocyclic compounds) [19]. The introduction of a heteroatom into the carbon ring reduces both the reaction enthalpy and the dehydrogenation temperature; however, a reduced storage capacity is expected with respect to its corresponding all-carbon counterparts [18,20].

LOHCs can be used for long-term storage without energy losses and transported over long distances, repurposing the existing oil infrastructure and easing the transition to the hydrogen economy. In fact, most LOHCs are safe and easy to handle and their physical properties resemble those of diesel [21]. The chemical and physical properties of ideal carriers have been studied [22,23], also with reference to toxicity [24] and the thermodynamic properties of the reversible hydrogenation/dehydrogenation reactions [25,26]. Dibenzyltoluene (DBT) [27,28] and N-ethylcarbazole (NEC) [29,30] are currently the most researched compounds, showing promising potentials for both large-scale energy transport and energy storage [31].

The weakest point of LOHC technologies is, by far, the need to supply energy to drive the dehydrogenation process, which potentially makes up the greatest cost component. If this energy requirement could be lowered, LOHCs could offer lower levelised costs of conversion and storage [7]. To do so, the reaction heat to fuel the dehydrogenation process must come from recovery heat: end-user demand and hydrogen release must be optimally integrated [32,33].

The heat demand to dehydrogenate the carrier is highly variable over time if no control strategy is implemented. This fluctuation is due to the dependence of the reaction rate's concentration on the reactants. Even if constant pressure and temperature conditions could be granted, the release process would gradually slow as more hydrogen has been discharged. At first, a high amount of hydrogen is released quickly, and then the process continues at a slower and steady pace for a medium to low Degree of Hydrogenation (DoH). For example, assuming operation from an initial DoH of 0.95 to a final DoH of 0.20 [34] the second-order release rate of NEC becomes 95% slower [35].

Since the reaction rate of dehydrogenation reactions depends on hydrogen pressure and temperature [35], strategies to control the otherwise highly-variable hydrogen flow rate must rely on either pressure or temperature control. Metal Hydrides (MHs) are characterised by a similar dependence of hydrogen release on pressure and temperature, although the pressure dependence follows, in this case, a Van't Hoff law [36]: therefore, the research conducted on MH systems can be a reference for devising control strategies applied to LOHC systems.

Currently, very few studies in the literature deal with how to control the hydrogen release from a LOHC system, and these studies refer to specific applications without discussing general controllability properties. For example, Bollmann et al. investigate the dehydrogenation of a LOHC using the exhaust gas of a methane-fuelled porous media burner and controlling the reaction through the temperature of the unit

by means of a PID controller acting on the burner [37]. A PI controller is implemented in another study to control the current generated by a Proton Exchange Membrane (PEM) fuel cell acting on the hydrogen release pressure [38], while in another study, hydrogen release is controlled through reactor temperature and LOHC pumping rate [39].

In contrast, control strategies for MH systems have been widely analysed and discussed. Cho et al. developed a comprehensive general approach to these control systems, taking into account the influence of the initial pressure, temperature and flow rate of the circulation water, the overall heat transfer coefficient and the volume fraction of the bed on the discharge rate. A PID controller was set in place to follow a periodic step function, and the controllability range was estimated in terms of operating time with respect to the control variables' set values [40]. The design of a predictive controller model of multiparametric types for MH reactors was also carried out and presented as a general framework [41]. A neuro-fuzzy PID control system was applied to an MH reactor, deploying a conventional PID control and a back-propagation learning mechanism [42]. Through step changes in the voltage input, a dynamical response in terms of the reactor's temperature and pressure is achieved with no overshoot and a reduced rising time with respect to a conventional PID controller. Later, a fuzzy PID control system was evaluated again with great emphasis on the control system design [43].

The similarity in the reaction rate equation between LOHCs and MHs makes it possible to devise control strategies for LOHC systems following the approach used in the previously mentioned studies on MH control systems. Therefore, the aim of this paper and its novel contribution to the literature is to provide an overall assessment of the controllability of LOHC systems acting within a general framework regardless of the specific application field. In particular, the control system is applied to a batch reactor with NEC used as the hydrogen carrier; the batch reactor is designed and modelled with a lumped-parameter approach devised by the authors [44]. Alternative control strategies are compared under different working conditions in terms of controllability time, that is, in terms of how long the system can supply the required hydrogen flow rate, which is a measure of the actual efficiency of the storage system under different loads. Research on the performance of control systems highlights the operational constraints of this technology. Relevant information on the controllability range and the energy-to-power ratio is deduced independently from the system size by scaling a constant power demand with respect to the uncontrolled release trend. Such a general approach is meant to serve as a preliminary guide for matching LOHC storage systems to specific applications, depending on the availability of controllability options and power demand.

Methods

Kinetic and thermodynamic model

LOHC systems rely on endothermic dehydrogenation reactions to release hydrogen. For a given catalyst, the reaction rate is determined by the concentration of the reactants and the thermodynamic conditions in terms of pressure and temperature:

$$r = k_0 f(p) g(T) z(\mathrm{DoH}) \tag{1}$$

The Degree of Hydrogenation DoH measures the amount of hydrogen still bound to the hydrogen carrier, and its rate of change (corresponding to the reaction rate) is thus related to the mass flow rate of hydrogen released through the following equation, where w is the maximum gravimetric density and M_{LOHC} is the LOHC's molar mass:

$$\dot{m}_{\mathrm{H_2},r} = w\, M_{\mathrm{LOHC}} \frac{\mathrm{dDoH}}{\mathrm{dt}} \tag{2}$$

The reaction rate can be expressed for the dehydrogenation of NEC systems as [35]:

$$\frac{\mathrm{dDoH}}{\mathrm{dt}} = -k_0 \exp(-bp) \exp\left(-\frac{E_a}{RT}\right) \mathrm{DoH}^2 \tag{3}$$

Thus, in the case of NEC, the reaction rate changes exponentially with pressure through a pressure coefficient b; it depends on temperature according to an Arrhenius-like factor; it follows a second-order reaction, depending on the DoH squared; finally, it is proportional to a reaction constant (k_0) that depends on the catalyst. The numerical values of the parameters used in this equation were presented in a previous work by the authors [44] and are reproduced in Table 1.

Since the reaction is endothermic, a heating source is needed to balance the heat sunk by the release; otherwise, the temperature drop would severely hinder the reaction kinetics. The energy balance can thus be written as follows:

$$C_T \frac{\mathrm{dT}}{\mathrm{dt}} = \varepsilon \dot{m}_f c_f (T_{f,in} - T) + \frac{\mathrm{d}m_{\mathrm{H_2}}}{\mathrm{dt}} (\Delta H_r + \Delta h - \Delta u) \tag{4}$$

with C_T being the overall heat capacity of the LOHC. In this equation, the heat rate transferred to the reactor $\dot{Q}_f = \varepsilon \dot{m}_f c_f (T_{f,in} - T)$ is a function of the heat transfer effectiveness ε, the Heat Transfer Fluid (HTF) mass flow rate $(\dot{m}_f)$ and specific heat (c_f), and the temperature difference between the HTF and the system. The reaction contribution to the energy balance is proportional to the released hydrogen mass flow rate and accounts for the reaction heat (ΔH_r) and the enthalpy differences (Δh) as hydrogen leaves the system at a given temperature — i.e. corresponding to the instantaneous LOHC temperature — while the last term accounts for differences in the internal energy of the system (Δu) due to the release [45].

Equations 3 and 4 make up the lumped-parameter model of a batch reactor, together with the equations that determine the heat transfer performance, in terms of heat transfer effectiveness ϵ and pressure losses on the HTF side, as detailed in a previous work by the authors [44].

Table 1 – Parameters defining the reaction rate (Eq. (3)).

Parameter	Value
k_0/s^{-1}	4.35×10^{10}
b/bar^{-1}	1.397
$E_a/(\mathrm{kJ/mol})$	121

Control system

In real-life applications, hydrogen release should follow the end user's demand. As such, the system's pressure, temperature, or both, must be controlled. A PI controller was thus introduced, and a Simulink/Simscape model was built, introducing a newly defined library for the LOHC system from the ground up. The schematic modelling used for the simulations is illustrated in Fig. 1. The heat exchange efficiency module relies on the procedure presented by the authors for a batch reactor [44] and calculates the heat transfer effectiveness based on the HTF velocity v_f and temperature T_f, together with the geometric data related to both the reactor and the HTF pipes. The heating system module then solves the energy balance of the reactor (Eq. (4)), while the hydrogen release module evaluates the mass flow rate of released hydrogen based on Eqs. (2) and (3).

Once a target hydrogen mass flow rate is defined on the basis of the user's load, the change between the actual instantaneous release and its target value is fed to PI controllers acting on release pressure, HTF inlet temperature, and HTF mass flow rate. The values of these parameters are obtained as the sum of a constant term and a correction, which is set to the respective PI output when that variable is chosen as the actual control variable or to zero when it is kept as a constant design parameter. A saturation block introduces reasonable limits to the allowed variations. In Fig. 1, pressure is chosen as the control parameter, as highlighted by the solid line of the switch connected to the correction dp obtained from the controller.

Three PI control logic procedures were introduced based on the control of the reactor pressure level, the inlet temperature of the HTF and its mass flow rate through control of the fluid's speed. For the latter, the instantaneous heat transfer effectiveness was evaluated to account for the different heat capacities and convection coefficients. Each control strategy was tested independently of the others. In the simulations, the control variables were first set at the reference values and then varied in the ranges given in Table 2.

Table 2 – Reference value and variability range for each control variable.

Control variable		Reference value	Range
Reactor pressure	p/bar	1.00	0.50–3.00
HTF inlet temperature	T_f/K	473	288–500
HTF velocity	v_f/(m/s)	2	0–5

Performance parameters

Two parameters were used to assess the controllability of the system. The first depends on the actual period of time ($t_{control}$) during which the system is able to supply the required hydrogen flow rate $\dot{m}_{target}$; the parameter t_R normalises this period of time with respect to the theoretical maximum release time τ, defined as the ratio of stored hydrogen $m_{H_2,stored}$ to the required flow rate:

$$\tau = m_{H_2,stored}/\dot{m}_{target} \tag{5}$$

$$t_R = \frac{t_{control}}{\tau} = \frac{m_{H_2,rel}}{m_{H_2,stored}} \tag{6}$$

The variable $m_{H_2,rel} = \dot{m}_{target} t_{control}$ represents the amount of hydrogen that the system can release at a constant mass flow rate thanks to the control system (neglecting the brief initial transient). Therefore, this normalised time t_R can be seen as a measure of the control system's efficiency, as the second definition in Eq. (6) clearly demonstrates.

The second parameter is the time delay t_D, after which the released mass flow rate reaches its target value. Thus, this parameter is not related to the efficiency of the controlled

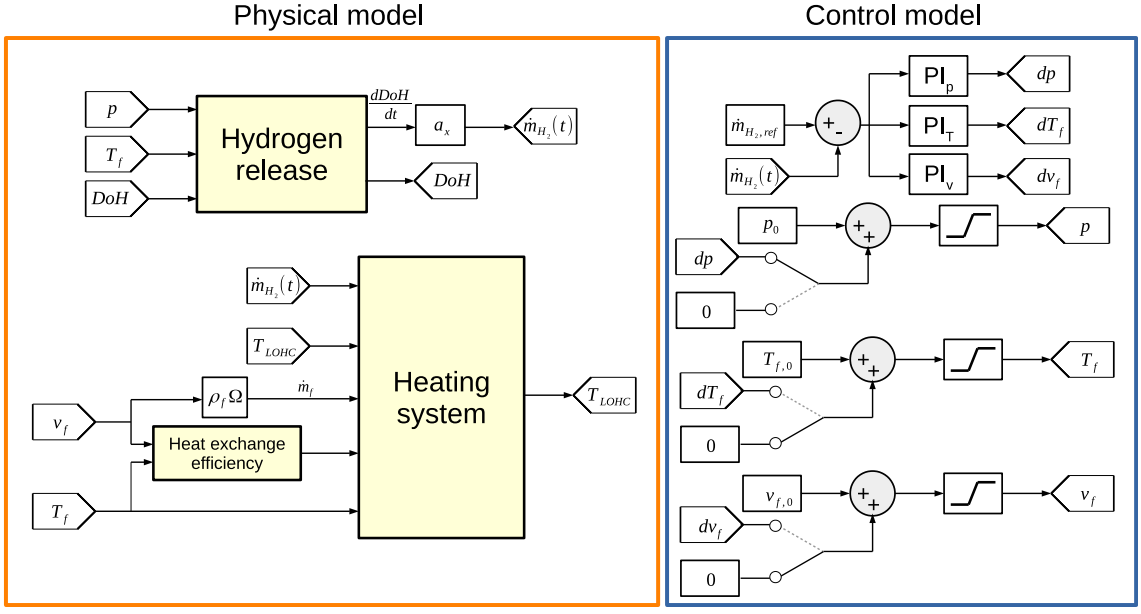

Fig. 1 – Schematic models of the heated reactor and the control apparatus.

system; it assesses how quickly the controlled system responds to user demand.

The time ratio t_R is independent of the storage size, so the results obtained are general and can be extended to storage systems of any size. However, a normalised measure of power must also be introduced to describe its effect on the time ratio in a size-independent way. To untie the influence of load on the controllability performance from the size of the system, a quantile analysis was performed on the uncontrolled mass release profile at constant pressure and temperature, which is represented in Fig. 2 for a net 5 kWh NEC system taking into account a fuel cell with an overall HHV-based efficiency of 0.45 [34], corresponding to 282 g of available hydrogen. At constant temperature and pressure, the reaction rate is solely determined by the second-order dependence on hydrogen concentration (Eq. (3)); a discussion about hydrogen release at constant operating conditions can be found in the literature [46,47]. The uncontrolled LOHC system provides a highly variable flow rate if kept at constant pressure and temperature: as Fig. 2 shows, the mass flow rate is reduced by more than 95% as the DoH decreases from 0.95 to 0.20.

The data on the flow rate time evolution were sorted and divided into ten intervals by deciles so that each group contained exactly one-tenth of the collected data. The power demand P, which is proportional to the required hydrogen flow rate $\dot{m}_{target}$, was then divided by the corresponding eighth-decile value so that the time ratio t_R and the time delay t_D can be represented against the normalised load $P/P_{8^{th}decile}$ to obtain a generalised assessment of the properties of the LOHC storage system, regardless of the size of the storage system.

Simulations were run for the third, fifth, seventh, and eighth deciles (represented as thin horizontal lines in Fig. 2) and the averaged mass flow rate value (bold line). The mean hydrogen release mass flow rate ($m_{H_2,released}/\Delta t$) falls between the seventh and eighth deciles. For more than 20% of the operating time, the flow rate would be higher, with a maximum of approximately five times higher. These results

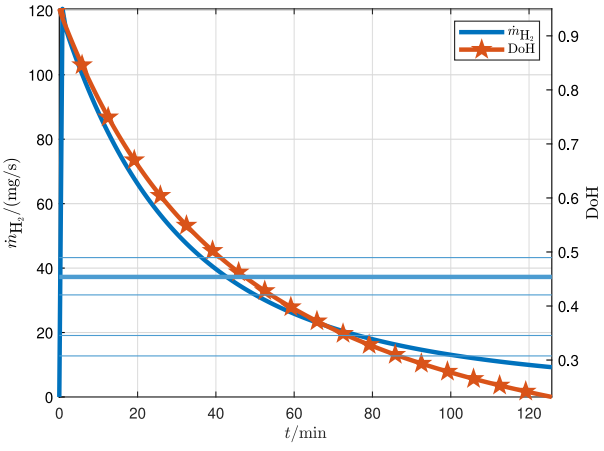

Fig. 2 – Mass flow rate and DoH over time at 473 K and 1 bar for the hydrogenated NEC sample. The bold line accounts for the mean release, while the thin lines represent the 3rd, 5th, 7th, and 8th deciles used in the simulations.

are consistent with the significantly faster release that occurs for high values of DoH.

The theoretical release time τ provides an alternative way to identify the load in a size-independent way if the energy content of the storage system is kept constant (clearly, the higher the load, the lower the theoretical release time). For the system represented in Fig. 2, the theoretical release time corresponding to the deciles considered in the simulation varies approximately in the range 2–6 h, as shown in Table 3.

Results and discussion

Theoretical performance under constant hydrogen release

Under the assumption of a constant rate of hydrogen release, the degree of hydrogenation would decrease linearly with time and the reaction rate (Eq. (3)) would be constant, as shown in the following equations, where x replaces DoH for simplicity of notation:

$$x(t) = x_0 - \dot{x}t \tag{7}$$

$$-k_0\exp(-bp)\exp\left(-\frac{E_a}{RT}\right)x(t)^2 = -\dot{x} \tag{8}$$

The reaction rate $\dot{x}$ can be determined as the ratio between the overall change in the degree of hydrogenation ($\Delta x = 0.75$) and the theoretical discharge time τ. So, for example, in the case of the averaged mass flow rate ($\tau = 2.1$ h), the reaction rate is $\dot{x} = \Delta x/\tau = 9.9 \times 10^{-5}\ s^{-1}$.

The previous equations show that the hydrogen pressure and temperature should change with time in the following way to maintain a constant rate of dehydrogenation:

$$\exp(-bp)\exp\left(-\frac{E_a}{RT}\right) = \frac{\dot{x}/k_0}{x(t)^2} \tag{9}$$

Therefore, the theoretical performance of the controlled system can be studied analytically in a straightforward way under the assumption that hydrogen pressure is constant if the reaction is controlled through the system temperature or that temperature is constant if pressure is taken as the control parameter.

In the latter case, setting the system temperature to its reference value $T_{ref} = 473$ K, hydrogen pressure should be varied by the control system according to the following equation:

$$p(t) = -b^{-1}\log\left(\frac{\dot{x}/k_T}{x(t)^2}\right) \tag{10}$$

Table 3 – Theoretical discharge time (energy-to-power ratios) for the deciles of power considered in the simulations, with 473 K and 1 bar as reference temperature and pressure.

Power decile	3rd	5th	7th	avg.	8th
τ/h	6.14	4.10	2.47	2.10	1.81

where $k_T = k_0 \exp(-E_a/(RT_{ref})) = 1.89 \times 10^{-3}$ s^{-1}. So, as hydrogenation decreases with time, the controller should decrease the hydrogen pressure proportionally to its logarithm: $p \propto 2b^{-1} \log x$.

On the other hand, if the system temperature is the control parameter, with the assumption of constant pressure ($p = p_{ref} = 1$ bar), the following equation is obtained:

$$T(t) = -\frac{E_a/R}{\log\left(\frac{\dot{x}/k_p}{x(t)^2}\right)} \tag{11}$$

where $k_p = k_0 \exp(-bp_{ref}) = 1.08 \times 10^{10}$ s^{-1}. This equation shows that, as hydrogenation decreases with time, the controller should act in such a way that the system temperature increases proportionally to the inverse of the logarithm of the degree of hydrogenation.

The variation with time of the theoretical values of pressure and temperature derived from Eqs. (10) and (11) is presented in the next section, compared to the actual values of hydrogen pressure and HTF inlet temperature obtained with the PI controller described in Section 2.2.

Control system performance

The effect of different loads on the controllability of the system is represented in Fig. 3, in terms of the time ratio t_R (Eq. (6)), which assesses the efficiency of the system, as discussed in the previous section. Setting reasonable bounds to the control variables range, higher power requirements can only be met for a limited time period, while lower requirements can be met for extended time periods, allowing for a deeper discharge. Due to controllability issues, a certain amount of hydrogen cannot be effectively released by the system, and its quantity depends on the power demand. The higher the target power, the higher the unreleased hydrogen content, since the contribution of z (DoH) in Eq. (1) is too low to be counterbalanced by variations in $f(p)$ or $g(T)$ in the given range of variability of the controlled variables.

As Fig. 3 shows, the HTF inlet temperature provides the most effective control over the entire power range since the largest amount of hydrogen can be released with the required mass flow rate: the efficiency is above 90% for power demands up to the 8th decile, that is, for energy-to-power ratios τ above approximately 1.8 h for the given reference thermodynamic conditions. Pressure control yields an adequate match for a low hydrogen demand but displays a sharper drop in efficiency as the power requirement increases: efficiency remains above 80% only for loads up to the 5th decile ($\tau \gtrsim 4$ h). Lastly, mass flow rate control is by far the least effective, as efficiency is at most 80% in all situations considered: hence, to keep the release rate above its low tail values, either a temperature or pressure increase is required. However, mass flow rate control is at its core a temperature control strategy that relies on a variable heat capacity to either increase or decrease the heat rate $\dot{Q}_f$, which is, however, still exchanged at the same temperature $T_{f,in,0}$. As such, even without an upper limit for v_f greater releases than those obtained in the constant temperature and pressure sample cannot be achieved.

In contrast, the time delays (Fig. 4) to reach the set value decrease with higher power levels according to the release curve, since the initial release is the highest and more limited restrictions are required. Temperature control is still the most effective, with an almost instantaneous theoretical response. Pressure control has a significantly higher but still low response time that ranges between 1 and 2 min. Mass flow rate control has the poorest reactivity, dramatically increasing at low loads since even the unheated system has a relatively high temperature.

These results can be explained in detail by looking at Fig. 5, which shows how the mass flow rate and the DoH change over time for the average mass flow rate ($\tau = 2.10$ h). The initial mass flow rate is significantly lowered to meet the targeted goal, and a constant release is maintained for a widely different time span depending on the control logic. Temperature control reaches the desired mass flow rate faster than the other strategies, resulting in a shorter time delay t_D as seen in Fig. 4, and keeps a steady supply for a longer period of time,

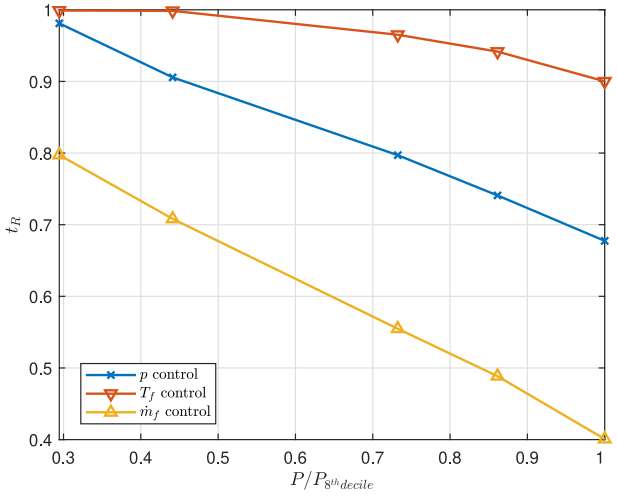

Fig. 3 – Relative time controllability for increasing values of power. Markers indicate the deciles considered in the simulation: 3rd, 5th, 7th, and 8th deciles.

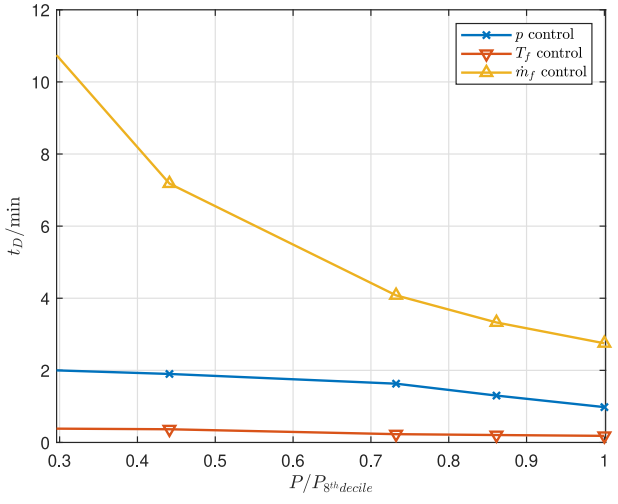

Fig. 4 – Time delay to reach the target power for increasing values of power. Markers indicate the deciles considered in the simulation: 3rd, 5th, 7th, and 8th deciles.

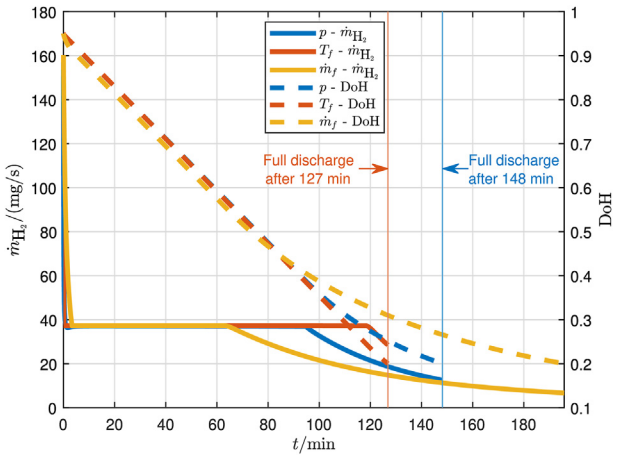

Fig. 5 – Hydrogen mass flow rate and DoH over time for the averaged mass flow rate target. In this figure numerical data are relative to a 5 kWh system.

resulting in a higher time ratio t_R as shown in Fig. 3. While, at first, the mass flow rate control has a slightly lower DoH due to a more pronounced delay to reach the target release, the DoH trends are mostly similar during the controllability range. When the DoH term in Eq. (3) gets too small, the system can no longer supply the required mass flow rate, so the curves corresponding first to the mass flow rate control and then to the pressure control deviate from the temperature-controlled system behaviour. A lower mass flow rate is released, resulting in higher levels of DoH.

Fig. 6 better explains why each control strategy deviates from the target mass flow rate at a specific time instant. Due to the finite variability range, once the respective bounds are reached, no further regulation margin is available to control the release. In particular, the time evolution of the hydrogen pressure (Fig. 6*a*), the HTF inlet temperature (Fig. 6*b*), and the HTF velocity (Fig. 6*c*) are presented for a target mass flow rate corresponding to the average value, as in Fig. 5.

In Fig. 6*a* pressure is shown to increase rapidly to limit the reaction rate, then it decreases steadily until the lower threshold is reached: consequently, the mass flow rate is shown to deviate from then on in Fig. 5. The pressure level set by the PI controller (solid line) is consistently lower than the theoretical value deduced from Eq. (10), mainly because the system temperature is generally lower than its reference value due to the endothermic nature of the dehydrogenation reaction; however, the shape of the curve is remarkably similar.

Fig. 6*b* shows how the HTF inlet temperature must change with time to return the desired result. An ambient-temperature mass flow rate is required first to cool off the reactor; then, the heating fluid must supply the reaction heat to fuel the release. A smooth increase is observed over time, saturating at the range's upper bound. The theoretical system temperature is shown for comparison, but it must be observed that the two curves are related to the temperature of two different systems: the HTF inlet temperature (solid line) and the hydrogen-LOHC system (thin line with markers). The HTF must obviously be hotter than the LOHC to be able to transfer the heat required to sustain the reaction, but the trend is the same that could be foreseen by means of Eq. (11).

Lastly, Fig. 6*c* shows how an increasingly higher mass flow rate is needed as time passes, obtained through an increased velocity of the thermal fluid. A secondary beneficial effect is also provided by the variation in heat transfer effectiveness due to a different v_f. After an initially smooth increase, the HTF flow rate that would be required to sustain the reaction at the required hydrogen discharge rate quickly increases due to the reduction in DoH, since the discharge rate depends on the square of this parameter (Eq. (3)). In particular, it is evident that even if the actual discrepancy with the target power occurs at $t \approx 67$ min, a substantial increase in velocity is needed from about $t \approx 50$ min, corresponding to DoH $\approx$0.65, to compensate for the reduction in the term z (DoH) in Eq. (1) through an increase in temperature. This result is consistent with Fig. 6*b*, as the required T_f increases above the reference temperature at approximately the same instant.

Further simulations were performed by changing the initial HTF inlet temperature by ±10 K and then increasing the working pressure to 1.25 bar, a value that could be more reasonable for a real batch system. Fig. 7 highlights how time controllability changes for different thermodynamic set

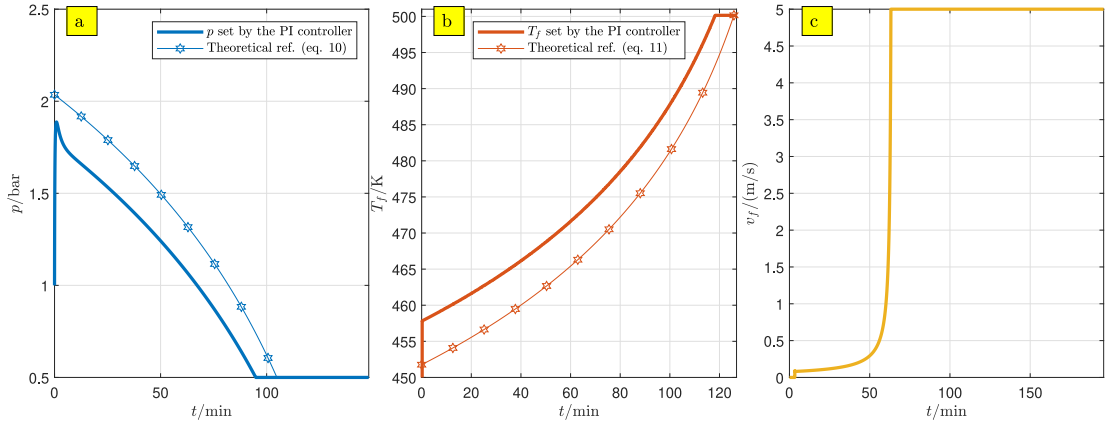

Fig. 6 – Pressure (a), HTF inlet temperature (b), and HTF velocity (c) variation over time for each respective control strategy.

points. Mass flow rate control is still the least effective. Slightly better performance is achieved for higher pressure levels, but with a greater influence of the set temperature. For low values, better utilisation is achieved since the reduced tail-end release requires a higher temperature in the reactor to reach the set power target. As such a high $T_{f,inlet}$ increase the effectiveness of a mass flow rate control. On the contrary, a 10 K temperature increase produces dramatically worse results, with less than 30% usage for the eighth decile. Pressure control benefits from higher set pressure levels since they provide a greater control margin at the tail end as the lower bound of the variability range is reached. The higher the temperature, the lower the effectiveness of the pressure control due to the greater influence of the temperature factor in Eq. (3). Lastly, temperature control yields slightly worse performance at high load and high pressure, since the pressure influence is more marked. A lower reference temperature benefits controllability performances as a greater $\Delta T_{f,inlet}$ is available to speed up the reaction. Similarly to mass flow rate control, the higher the set level, the lower the effectiveness with a sharp decrease related to the need to raise the temperature level above its set value to improve kinetics at low DoH.

The various time delays are represented in Fig. 8 with respect to the power demand and the thermodynamic conditions. Temperature control is still almost instantaneously tuned to the set value for every simulation scenario. A more variable trend is showcased by pressure control, with a reduced delay time for high-temperature and low-pressure simulations. However, mass flow rate control has a widely variable reactivity. Since the initial regulation requires a dramatic reduction in release, this time high-temperature values speed up the process as the PI controller establishes a null mass flow rate. High pressure levels are again related to longer time delays. Regardless, mass flow rate control is still definitely the least convenient option.

Therefore, the sensitivity analysis reaffirms the whole temperature control strategy as the best fit to enhance controllability throughout the power range. Even though the

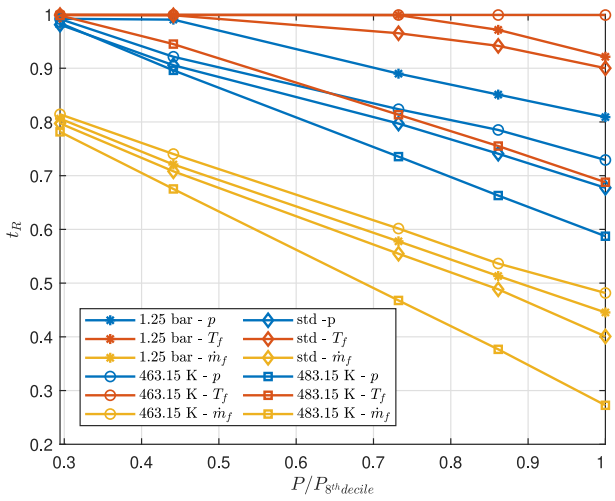

Fig. 7 – Relative time controllability for different control logic at various thermodynamic set points.

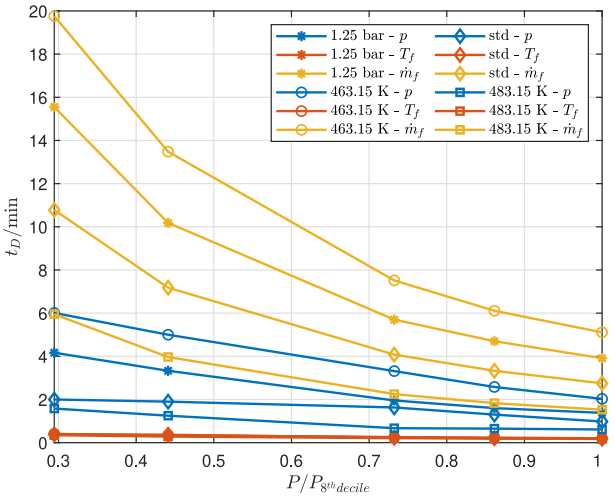

Fig. 8 – Time delay for different control logic at various thermodynamic set points.

set variability ranges of pressure and temperature moving from the lower to the upper bound lead to a 500.0% and 73.6% (considering the inverse of the temperature due to Eq. (3)) increase, the 121.0 kJ/mol activation energy and the 1.397 bar^{-1} pressure coefficient [44] give temperature a relatively more marked influence over the kinetic rate.

In general, when using temperature or pressure as control parameters, a power demand equal to or less than the fifth decile can be met with relatively high efficiencies (90% or above). Unless a high reference temperature is needed, for example if a high release rate is sought, such efficiencies can be reached with temperature as the control parameter even for higher loads.

Although the importance of heat recovery for the competitiveness of LOHC-based storage systems cannot be understated, the required high-temperature heat sources might prove difficult to find, limiting the possible applications of this storage technology. So, even though changing the HTF inlet temperature has been shown to be the most effective way to control the release process, the temperature of the heat source could significantly restrict the range of variability for this control parameter. However, the enthalpy change of the dehydrogenation reaction is less than 20% of hydrogen's HHV [44], so it is the quality of the available waste heat (the temperature of the heat source) rather than its quantity that represents the main constraint on the feasibility of this technology. Moreover, in most applications the HTF inlet temperature would be determined by the performance of a recovery heat exchanger where waste heat is recovered, and the heat exchanger dynamics should be taken into account in the model of a specific application. Similarly, both low- and high-pressure levels are challenging because of storage-to-user coupling and the need for hydrogen compression. Therefore, a multiparameter approach could be introduced to increase the controllability or limit the respective variability range, or both. Moderate regulation of the mass flow rate could be studied as a support control strategy; however, the

sensitivity analysis highlighted its poor performance when a medium-low DoH is reached.

Conclusions

LOHC systems are characterised by a non-constant hydrogen release over time unless control strategies are put in place. This is necessary to couple hydrogen storage to end-user demand. Different control strategies can be implemented to influence the kinetic rate, acting on the temperature and pressure of the reactor. For a given size and reasonable ranges of variability for each control variable, a maximum controllability time can be defined with respect to the power demand; this parameter identifies the system storage efficiency under different loads, as it measures the actual amount of hydrogen released against the stored hydrogen. In this paper, different constant demand values were considered and defined by decile analysis to allow for general considerations. Practical values of theoretical release time, corresponding to the energy-to-power ratio, are found in the interval 2–6 h for LOHC systems.

Regarding the feasibility of each control strategy, the temperature control shows the best results: efficiency remains above 90% over the entire range of loads considered, that is, for energy-to-power ratios τ as low as 1.5–2.0 h; pressure control only leads to satisfactory performance at low load ($\tau \gtrsim 4$ h). Although easier to implement, mass flow rate control alone shows a lacklustre controllability, resulting in an efficiency below 80% over the whole load range considered, and both controllability and delay times are significantly worse than those achieved with different control strategies.

Although temperature control allows for over 90% discharge even for the eighth decile, pressure control leads to similar performances for lower-than-median loads. On the other hand, the energy stored is fully released at a load corresponding to the fifth decile ($\tau \approx 4$ h) with temperature control. As such, this energy-to-power ratio could identify the best power level to operate the reactor as the best trade-off between storage efficiency and power output.

Under different reference thermodynamic conditions, temperature control is still the most effective, losing effectiveness only if higher reference temperature levels are required. Consistently lower but overall adequate performances are achieved through pressure control, again suffering the influence of a higher temperature. Mass flow rate control remains the least reliable control logic, dramatically losing effectiveness for higher temperature.

More complex control strategies could be investigated, introducing a synergistic multi-parameter control to make use of the good controllability of pressure and temperature while reducing the strain in the required variation range.

CRediT authorship contribution statement

Marco Gambini: Validation, Visualisation. **Federica Guarnaccia:** Conceptualisation, Methodology, Software, Validation, Writing - Original Draft, Writing - Review & Editing, Visualisation. **Michele Manno:** Conceptualisation, Methodology, Validation, Writing - Original Draft, Writing - Review & Editing, Visualisation, Supervision. **Michela Vellini:** Validation, Visualisation.

Declaration of competing interest

The authors declare that they have no known competing financial interests or personal relationships that could have appeared to influence the work reported in this paper.

Nomenclature

c	specific heat (J/(kg K))
C_T	heat capacity (J/(kg K))
ΔH_r	reaction enthalpy change (J/kg)
E_a	activation energy (J/(mol K))
h	specific enthalpy (J/kg)
k_0	pre-exponential factor (mol/s)
m	mass (kg)
$\dot{m}$	mass flow rate (kg/s)
M	molar mass (kg/mol)
P	power (W)
p	pressure (Pa)
$\dot{Q}$	heat rate (W)
r	reaction rate (mol/s)
R	universal gas constant (8.3145 J/(mol K))
t	time (s)
T	temperature (K)
u	specific internal energy (J/kg)
v	velocity (m/s)
w	gravimetric storage capacity (–)

Greek letters

ϵ	heat exchanger effectiveness (–)

Subscripts

D	delay
f	heat transfer fluid
R	ratio

Acronyms

DBT	DiBenzylToluene
DoH	Degree of Hydrogenation
HHV	Higher Heating Value
HTF	Heat Transfer Fluid
LOHC	Liquid Organic Hydrogen Carrier
MH	Metal Hydride
NEC	N-EthylCarbazole
PEM	Proton Exchange Mebrane (Fuel Cell)
PID	Proportional Integral Derivative (controller)
RES	Renewable Energy Source

REFERENCES

[1] International Energy Agency Renewables 2022. Analysis and forecast to 2027. 2023. https://www.iea.org/reports/renewables-2022.

[2] Sterner M, Specht M. Power-to-Gas and power-to-X—the history and results of developing a new storage concept.

Energies 2021;14(20):6594. https://doi.org/10.3390/en14206594.
[3] International Renewable Energy Agency. Innovation landscape for a renewable-powered future: solutions to integrate variable renewables. 2019. https://www.irena.org/-/media/Files/IRENA/Agency/Publication/2019/Feb/IRENA_Innovation_Landscape_2019_report.pdf.
[4] Nastasi B. Power to Gas and Hydrogen applications to energy systems at different scales – building, District and National level. Int J Hydrogen Energy 2019;44(19):9485. https://doi.org/10.1016/j.ijhydene.2019.02.197 [Special Issue on Power To Gas and Hydrogen applications to energy systems at different scales – Building, District and National level.].
[5] International Renewable Energy Agency. Innovation landscape brief: renewable power-to-hydrogen. 2019. https://www.irena.org/-/media/Files/IRENA/Agency/Publication/2019/Sep/IRENA_Power-to-heat_2019.pdf.
[6] Deloitte. Investing in hydrogen: ready, set, net zero. 2020. https://www2.deloitte.com/content/dam/Deloitte/uk/Documents/energy-resources/deloitte-uk-energy-resources-investing-in-hydrogen.pdf. [Accessed 7 February 2023].
[7] Deloitte. The potential of hydrogen for the chemical industry. 2021. https://www2.deloitte.com/content/dam/Deloitte/xe/Documents/energy-resources/me_pov-hydrogen-chemical-industry.pdf. [Accessed 7 February 2023].
[8] Proost J. State-of-the art CAPEX data for water electrolysers, and their impact on renewable hydrogen price settings. Int J Hydrogen Energy 2019;44(9):4406–13. https://doi.org/10.1016/j.ijhydene.2018.07.164.
[9] Skordoulias N, Koytsoumpa EI, Karellas S. Techno-economic evaluation of medium scale power to hydrogen to combined heat and power generation systems. Int J Hydrogen Energy 2022;47(63):26871–90. https://doi.org/10.1016/j.ijhydene.2022.06.057.
[10] Genovese M, Schlüter A, Scionti E, Piraino F, Corigliano O, Fragiacomo P. Power-to-hydrogen and hydrogen-to-X energy systems for the industry of the future in Europe. Int J Hydrogen Energy 2023. https://doi.org/10.1016/j.ijhydene.2023.01.194.
[11] Us Department of Energy. Hydrogen storage. 2023. https://www.energy.gov/eere/fuelcells/hydrogen-storage. [Accessed 7 February 2023].
[12] Barthelemy H, Weber M, Barbier F. Hydrogen storage: recent improvements and industrial perspectives. Int J Hydrogen Energy 2017;42(11):7254–62. https://doi.org/10.1016/j.ijhydene.2016.03.178.
[13] Ustolin F, Campari A, Taccani R. An extensive review of liquid hydrogen in transportation with focus on the maritime sector. J Mar Sci Eng 2022;10(9):1222. https://doi.org/10.3390/jmse10091222.
[14] Products Air. Liquid hydrogen: safetygram 9. 2021. https://www.airproducts.com/-/media/airproducts/files/en/900/900-13-082-us-liquid-hydrogen-safetygram-9.pdf. [Accessed 7 February 2023].
[15] Petitpas G. Boil-off losses along LH2 pathway. Technical report, Lawrence Livermore National Laboratory 2018. https://www.osti.gov/servlets/purl/1466121.
[16] Preuster P, Papp C, Wasserscheid P. Liquid organic hydrogen carriers (LOHCs): toward a hydrogen-free hydrogen economy. Energy Environ Sci 2008;1(1):134–8. https://doi.org/10.1021/acs.accounts.6b00474.
[17] Caglayan DG, Heinrichs HU, Robinius M, Stolten D. Robust design of a future 100% renewable European energy supply system with hydrogen infrastructure. Int J Hydrogen Energy 2021;46(57):29376–90. https://doi.org/10.1016/j.ijhydene.2020.12.197.
[18] Bourane A, Elanany M, Pham TV, Katikaneni SP. An overview of organic liquid phase hydrogen carriers. Int J Hydrogen Energy 2016;41(48):23075–91. https://doi.org/10.1016/j.ijhydene.2016.07.167.
[19] Stepanenko SA, Shivtsov DM, Koskin AP, Koskin IP, Kukushkin RG, Yeletsky PM, Yakovlev VA. N-heterocyclic molecules as potential liquid organic hydrogen carriers: reaction routes and dehydrogenation efficacy. Catalysts 2022;12(10). https://doi.org/10.3390/catal12101260.
[20] Crabtree RH. Hydrogen storage in liquid organic heterocycles. Acc Chem Res 2017;50(1):74–85. https://doi.org/10.1021/acs.accounts.6b00474.
[21] Eypasch M, Schimpe M, Kanwar A, Hartmann T, Herzog S, Frank T, Hamacher T. Model-based techno-economic evaluation of an electricity storage system based on Liquid Organic Hydrogen Carriers. Appl Energy 2017;185(1):320–30. https://doi.org/10.1016/j.apenergy.2016.1.
[22] Rao PC, Yoon M. Potential liquid-organic hydrogen carrier (lohc) systems: a review on recent progress. Energies 2020;13(22):6040. https://doi.org/10.3390/en13226040.
[23] Otto M, Chagoya KL, Blair RG, Hick SM, Kapat JS. Optimal hydrogen carrier: holistic evaluation of hydrogen storage and transportation concepts for power generation, aviation, and transportation. J Energy Storage 2022;55:105714. https://doi.org/10.1016/j.est.2022.105714.
[24] Markiewicz M, Zhang Y-Q, Empl MT, Lykaki M, Thöming J, Steinberg P, Stolte S. Hazard assessment of quinaldine-, alkylcarbazole-, benzene- and toluene-based liquid organic hydrogen carrier (LOHCs) systems. Energy Environ Sci 2019;12:366–83. https://doi.org/10.1039/C8EE01696H.
[25] von Wild J, Friedrich T, Cooper A, Toseland B, Muraro G, TeGrotenhuis W, Wang Y, Humble P, Karim A. Liquid Organic Hydrogen Carriers (LOHC): an auspicious alternative to conventional hydrogen storage technologies. In: Stolten D, Grube T, editors. Proceedings of the 18th world hydrogen energy conference 2010-WHEC; 2010. volume 78 of *Schriften des Forschungszentrums Jülich/Energy & Environment*, pages 189–197, Essen, 2010. ISBN 978-3-89336-654-5, https://juser.fz-juelich.de/record/135562/files/HS2b_2_von-Wild.pdf.
[26] Cooper A, Campbell K, Pez G. An integrated hydrogen storage and delivery approach using organic liquid-phase carriers. In *16th world hydrogen energy conference (WHEC)*. 2006.
[27] Dürr S, Zilm S, Geißelbrecht M, Müller K, Preuster P, Bösmann A, Wasserscheid P. Experimental determination of the hydrogenation/dehydrogenation – equilibrium of the LOHC system H0/H18-dibenzyltoluene. Int J Hydrogen Energy 2021;46(64):32583–94. https://doi.org/10.1016/j.ijhydene.2021.07.119.
[28] Park S, Naseem M, Lee S. Experimental assessment of perhydro-dibenzyltoluene dehydrogenation reaction kinetics in a continuous flow system for stable hydrogen supply. Materials 2021;14(24):7613. https://doi.org/10.3390/ma14247613.
[29] Heublein N, Stelzner M, Sattelmayer T. Hydrogen storage using liquid organic carriers: equilibrium simulation and dehydrogenation reactor design. Int J Hydrogen Energy 2020;45(46):24902–16. https://doi.org/10.1016/j.ijhydene.2020.04.274.
[30] Kiermaier S, Lehmann D, Bösmann A, Wasserscheid P. Dehydrogenation of perhydro-N-ethylcarbazole under reduced total pressure. Int J Hydrogen Energy 2021;46(29):15660–70. https://doi.org/10.1016/j.ijhydene.2021.02.128.
[31] Niermann M, Beckendorff A, Kaltschmitt M, Bonhoff K. Liquid organic hydrogen carrier (LOHC) – assessment based on chemical and economic properties. Int J Hydrogen Energy 2019;44(13):6631–54.
[32] Dennis J, Bexten T, Petersen N, Wirsum M, Preuster P. Model-based analysis of a liquid organic hydrogen carrier (LOHC) system for the operation of a hydrogen-fired gas turbine. J

Eng Gas Turbines Power 2021;143:031011. https://doi.org/10.1115/1.4048596.
[33] Rüde T, Lu Y, Anschütz L, Blasius M, Wolf M, Preuster P, Wasserscheid P, Geißelbrecht M. Performance of continuous hydrogen production from perhydro benzyltoluene by catalytic distillation and heat integration concepts with a fuel cell. Energy Technol 2022;11(3):2201366. https://doi.org/10.1002/ente.202201366.
[34] Peters R, Deja R, Fang Q, Nguyen VN, Preuster P, Blum L, Wasserscheid P, Stolten D. A solid oxide fuel cell operating on liquid organic hydrogen carrier-based hydrogen – a kinetic model of the hydrogen release unit and system performance. Int J Hydrogen Energy 2019;44(26):13794–806. https://doi.org/10.1016/j.ijhydene.2019.03.220.
[35] Gambini M, Guarnaccia F, Di Vona ML, Manno M, Vellini M. Liquid organic hydrogen carriers: development of a thermodynamic and kinetic model for the assessment of hydrogenation and dehydrogenation processes. Int J Hydrogen Energy 2022;47(65):28034–45. https://doi.org/10.1016/j.ijhydene.2022.06.120.
[36] Gambini M, Manno M, Vellini M. Numerical analysis and performance assessment of metal hydride-based hydrogen storage systems. Int J Hydrogen Energy 2008;33(21):6178–87. https://doi.org/10.1016/j.ijhydene.2008.08.006.
[37] Bollmann J, Schmidt N, Beck D, Preuster P, Zigan L, Wasserscheid P, Will S. A path to a dynamic hydrogen storage system using a liquid organic hydrogen carrier (LOHC): burner-based direct heating of the dehydrogenation unit. Int J Hydrogen Energy 2023;48(3):1011–23. https://doi.org/10.1016/j.ijhydene.2022.09.234.
[38] Geiling J, Steinberger M, Ortner F, Seyfried R, Nuß A, Uhrig F, Lange C, Öchsner R, Wasserscheid P, März M, Preuster P. Combined dynamic operation of PEM fuel cell and continuous dehydrogenation of perhydro-dibenzyltoluene. Int J Hydrogen Energy 2021;46(72):35662–77. https://doi.org/10.1016/j.ijhydene.2021.08.034 [Special Issue on HYPOTHESIS XV].
[39] Fikrt A, Brehmer R, Milella V-O, Müller K, Bösmann A, Preuster P, Alt N, Schlücker E, Wasserscheid P, Arlt W. Dynamic power supply by hydrogen bound to a liquid organic hydrogen carrier. Appl Energy 2017;194:1–8. https://doi.org/10.1016/j.apenergy.2017.02.070.
[40] Cho J-H, Yu S-S, Kim M-Y, Kang S-G, Lee Y-D, Ahn K-Y, Ji H-J. Dynamic modeling and simulation of hydrogen supply capacity from a metal hydride tank. Int J Hydrogen Energy 2013;38:8813–28. https://doi.org/10.1016/j.ijhydene.2013.02.142.
[41] Panos C, Kouramas KI, Georgiadis MC, Pistikopoulos EN. Dynamic optimization and robust explicit model predictive control of hydrogen storage tank. Comput Chem Eng 2010;34:1341–7. https://doi.org/10.1016/j.compchemeng.2010.02.018.
[42] Nuchkrua T, Leephakpreeda T. Neuro-fuzzy adaptive PID control of thermoelectric module for metal hydride reactor. Defect Diffusion Forum 2013;334–335:182–1878. 10.4028/www.scientific.net/ddf.334-335.182.
[43] Aruna R, Jaya Christa ST. Modeling, system identification and design of fuzzy pid controller for discharge dynamics of metal hydride hydrogen storage bed. Int J Hydrogen Energy 2020;45:4703–19. https://doi.org/10.1016/j.ijhydene.2019.11.238.
[44] Gambini M, Guarnaccia F, Manno M, Vellini M. Thermal design and heat transfer optimisation of a Liquid Organic Hydrogen Carrier batch reactor for hydrogen storage. Preprint submitted to the International Journal of Hydrogen Energy, special issue SDEWES conference 2023;2022. https://doi.org/10.5281/zenodo.7624671.
[45] Gambini M. Metal hydride energy systems performance evaluation. Part A: dynamic analysis model of heat and mass transfer. Int J Hydrogen Energy 1994;19(1):67–80. https://doi.org/10.1016/0360-3199(94)90179-1.
[46] Dong Y, Yang M, Mei P, Li C, Li L. Dehydrogenation kinetics study of perhydro-N-ethylcarbazole over a supported Pd catalyst for hydrogen storage application. Int J Hydrogen Energy 2016;41(20):8498–505. https://doi.org/10.1016/j.ijhydene.2016.03.157.
[47] Feng Z, Bai X. 3D-mesoporous KIT-6 supported highly dispersed Pd nanocatalyst for dodecahydro-N-ethylcarbazole dehydrogenation. Microporous Mesoporous Mater 2022. https://doi.org/10.1016/j.micromeso.2022.111789.